Published in final edited form as:
Biochemistry. 2013 August 27; 52(34): 5928–5940. doi:10.1021/bi401019h.

Structural Mutations that Probe the Interactions between the Catalytic and Dianion Activation Sites at Triosephosphate Isomerase‡

Xiang Zhai[†], **Tina L. Amyes**[†], **Rik K. Wierenga**[§], **J. Patrick Loria**[#], and **John P. Richard**[*,†]

[†]Department of Chemistry, University at Buffalo, Buffalo, NY 14260, USA [§]Department of Biochemistry and Biocenter Oulu, University of Oulu, P.O. Box 3000, FIN-90014, Oulu, Finland [#]Department of Chemistry and Department of Molecular Biophysics and Biochemistry, Yale University, New Haven, CT 06520, USA

Abstract

Triosephosphate isomerase (TIM) catalyzes the isomerization of dihydroxyacetone phosphate to form D-glyceraldehyde 3-phosphate. The effects of two structural mutations at TIM on the kinetic parameters for catalysis of the reaction of the truncated substrate glycolaldehyde (GA) and the activation of this reaction by phosphite dianion are reported. The P168A mutation results in similar 50-fold and 80-fold decreases, respectively, in $(k_{cat}/K_m)_E$ and $(k_{cat}/K_m)_{E\cdot HPi}$ for deprotonation of GA catalyzed by free TIM and by the TIM•HPO_3^{2-} complex. The mutation has little effect on the observed and intrinsic phosphite dianion binding energy, or on the magnitude of phosphite dianion activation of TIM for catalysis of deprotonation of GA. A loop 7 replacement mutant (L7RM) of TIM from chicken muscle was prepared by substitution of the archaeal sequence 208-TGAG for 208-YGGS. The L7RM exhibits a 25-fold decrease in $(k_{cat}/K_m)_E$ and a larger 170-fold decrease in $(k_{cat}/K_m)_{E\cdot HPi}$ for reactions of GA. The mutation has little effect on the observed and intrinsic phosphodianion binding energy, and only a modest effect on phosphite dianion activation of TIM. The observation that both the P168A and loop 7 replacement mutations affect mainly the kinetic parameters for TIM-catalyzed deprotonation, but result in much smaller changes in the parameters for enzyme activation by phosphite dianion provide support for the conclusion that catalysis of proton transfer and dianion activation of TIM take place at separate, weakly interacting, sites in the protein catalyst.

INTRODUCTION

Triosephosphate isomerase (TIM) catalyzes the stereospecific and reversible conversion of dihydroxyacetone phosphate (DHAP) to (*R*)-glyceraldehyde 3-phosphate (GAP),[1,2] by a proton transfer mechanism through enzyme-bound *cis*-enediolate reaction intermediates (Scheme 1). The carboxylate anion side-chain of Glu165/167[a] functions as a Brønsted base

‡This work was supported by Grant GM 039754 from the National Institutes of Health.

*Author to whom correspondence should be addressed: Phone: (716) 645 4232, Fax: (716) 645 6963, jrichard@buffalo.edu.

SUPPORTING INFORMATION

Table S1: Rate constants and fractional product yields for the reaction of [1-^{13}C]-GA catalyzed by wildtype *c*TIM. Tables S2 and S3: Fractional product yields for the reaction of [1-^{13}C]-GA catalyzed by the loop 7 replacement mutant of TIM from chicken muscle and the P168A mutant of *Tbb*TIM. This material is available free of charge via the Internet at http://pubs.acs.org.

[a]We note the following small differences in the numbering of amino acid residues at TIM from chicken muscle and TIM from *Trypanosoma brucei brucei*, (*c*TIM/*Tbb*TIM): Glu165/Glu167; Pro166/Pro168; Pro166 to Ala176/Pro168 to Ala178 (loop 6); Tyr208 to Ser211/Tyr210 to Ser213 (loop 7).

to abstract a proton from the α-carbonyl carbon of bound substrate,[3–6] and the developing negative charge at the carbonyl carbon is stabilized by hydrogen bonding to the neutral imidazole side-chain of His-95.[7–9] The isomerization reaction is completed by reprotonation of the enediolate intermediate at the adjacent carbon (Scheme 1).

The results of more than 50 years of studies on triosephosphate isomerase (TIM) have served to define what is known about the mechanism for enzymatic catalysis of deprotonation of carbon, and the important problems that remain to be resolved. [1,10–14] It was suggested that catalysis by TIM is "not different, just better" than catalysis by small molecules.[15] TIM is "better" than small molecules in the sense that the catalytic side chains of TIM are activated for catalysis at the enzyme active site.[16–21] The 11-residue (166 – 176)[a] flexible phosphodianion gripper loop 6 of TIM from chicken muscle (*c*TIM) plays an important role in enzyme activation.[22–26] Loop 6 is open at unliganded TIM, allowing substrate access to the enzyme active site. The binding of substrate to TIM is followed by loop closure that sequesters the ligand from interaction with solvent water, and strips several solvent molecules from the enzyme active site.[27] The closure of loop 6 is accompanied by a conformational change of loop 7 and this loop closure is driven energetically by formation of hydrogen bonds between the backbone amides of Gly171 of loop 6 and of Ser211 of loop 7 to the ligand phosphodianion, along with the formation of interloop hydrogen bonds between loop 6 and the 208-YGGS motif of loop 7.[27–29]

Two experiments provide reinforcing pieces of evidence that interactions between the loop 6 of TIM and the substrate phosphodianion activate TIM for catalysis of isomerization.

1. Truncation of residues Ile170 - Gly173 at the tip of loop 6 of *c*TIM and the introduction of a peptide bond between Ala169 and Lys174 disrupts loop-phosphodianion interactions, but should not affect the protein fold.[22] The 10^5-fold decrease in k_{cat}, and much smaller 2.3-fold increase in K_m determined for isomerization of GAP catalyzed by this loop deletion mutant of *c*TIM shows that the full loop 6 is required to observe robust turnover of bound substrate.
2. Truncation of the phosphodianion from GAP leads to a 10^9-fold reduction in k_{cat}/K_m for TIM-catalyzed isomerization of the minimal neutral substrate glycolaldehyde (GA).[30] The binding of phosphite dianion to TIM results in a ca. 1000-fold increase in the catalytic activity of TIM toward towards deprotonation of GA.[30] A comparison of the TIM-catalyzed reactions of the whole substrate GAP and the substrate pieces shows that 50% of the total 11 kcal/mol intrinsic binding energy of the phosphodianion of GAP may be *recovered* as phosphite dianion activation of the reaction of GA.[30]

The determination of the mechanism for phosphite dianion activation of TIM is a difficult and significant problem, whose solution is broadly relevant to the mechanism of phosphite dianion activation of several enzymatic reactions, including enzyme-catalyzed decarboxylation,[31] proton transfer,[32,33] hydride transfer,[34] phosphoryl transfer,[35] and reductoisomerization reactions,[36] and to the more general problem of the mechanism for the utilization of the intrinsic substrate binding energy in stabilizing the transition states for enzymatic reactions.[37,38] We report here the results of a study of the effect of two structural mutations of TIM on enzyme activation by phosphite dianion.

The 208-YGGS sequence at residues 208 – 211 is generally observed for loop 7 of TIM.[29] The 208-TGAG sequence commonly found at archaeal organisms has been substituted for 208-YGGS at *c*TIM and the resulting loop 7 replacement mutant (L7RM) *c*TIM exhibits a 200-fold decrease in k_{cat}/K_m for isomerization of GAP and DHAP.[28] TROSY-Hahn Echo[39] and TROSY-selected R_{1p}[40] experiments indicate that this mutation of loop 7 results in a doubling in the rate of conformational exchange associated with active site loop motion, and

a reduction in the coordinated motion of loop 6 relative to that of wildtype TIM.[28] These results provide evidence that interactions between loop 6 and loop 7 are necessary to ensure the proper chemical environment for the enzymatic reaction; and, that interloop interactions play a significant role in modulating the chemical dynamics near the active site.[28] The P168A mutant of TIM from *Trypanosoma brucei brucei* (*Tbb*TIM) was targeted for study, because of the expectation that the excellent high-resolution X-ray crystal structures for free and liganded P168A mutant enzyme would provide a structure-based rationalization for the effect of the mutation on the kinetic parameters for enzyme activation by phosphite dianion.[41]

We report here that the 208-TGAG for 208-YGGS loop 7 replacement mutation of *c*TIM, and the P168A mutation of *Tbb*TIM result in decreases in the kinetic parameters for enzyme-catalyzed deprotonation of [1-^{13}C]-GA in the absence and in the presence of HPO_3^{2-} that are similar to the ca. 100-fold decreases in k_{cat} for the reaction of the whole substrate GAP. Both the P168A and loop 7 replacement mutant enzyme-catalyzed reactions of [1-^{13}C]-GA are strongly activated by phosphite dianion, and the activation is similar to that for the corresponding wildtype enzyme. The observation that these structural mutations cause a significant decrease in the reactivity of TIM toward catalysis of deprotonation of [1-^{13}C]-GA, but have little effect on enzyme activation by phosphite dianion, shows that it is possible to modify the catalytic activity at the site that carries out carbon deprotonation *without* severely affecting enzyme activation at the dianion binding site. These results provide new insight into the mechanism for enzyme activation.

EXPERIMENTAL

Materials

Rabbit muscle α-glycerol 3-phosphate dehydrogenase and glyceraldehyde 3-phosphate dehydrogenase was purchased from Sigma. These enzymes were exhaustively dialyzed against 20 mM triethanolamine buffer (pH 7.5) at 7 °C prior to use in coupled enzyme assays. Bovine serum albumin was purchased from Roche. DEAE Sepharose Fast Flow was purchased from GE Healthcare. D,L-Glyceraldehyde 3-phosphate diethyl acetal (barium salt), dihydroxyacetone phosphate (lithium salt), NADH (disodium salt), Dowex 50WX4-200R, triethanolamine hydrochloride and imidazole were purchased from Sigma. Hydrogen arsenate heptahydrate and sodium phosphite (dibasic, pentahydrate) were purchased from Fluka and were dried under vacuum prior to use.[30] [1-^{13}C]-Glycolaldehyde (99% enrichment of ^{13}C at C-1, 0.09 M in water) was purchased from Omicron Biochemicals. Deuterium oxide (99% D) and deuterium chloride (35% w/w, 99.9% D) were purchased from Cambridge Isotope Laboratories. Sodium 2-phosphoglycolate was synthesized by following a published procedure.[42] Imidazole was recrystallized from benzene. All other chemicals were reagent grade or better and were used without further purification.

Preparation of Enzymes

Expression vectors (pET-15b) containing genes coding for wildtype and L7RM *c*TIM were available from a previous study.[28] These plasmids were introduced into the TIM-deficient *tpi*A$^-$ λDE3 lysogenic strain of *E. coli*, FB215471(DE3), which was a generous gift from Professor Brian Miller.[43] Cells were grown overnight at 37 °C in 200 – 300 mL of Luria Broth that contained 100 μg/mL ampicillin and 40μg/mL kanamycin. These cultures were diluted into 6 L of the same medium and incubated at 37 °C until an OD_{600} of 0.6 was obtained. Protein expression was then induced by the addition of 0.6 mM isopropyl 1-thio-D-galactoside (IPTG) followed by incubation for an additional 6 h. The cells were harvested and suspended in 25 mM Tris-HCl at pH 8.0 (25 mL) and were stored at −80 °C. The

wildtype and L7RM *c*TIMs were purified according to a published procedure.[44] Fractions from the final DEAE Sepharose ion exchange column that were judged to be homogeneous by gel electrophoresis were pooled, concentrated, and stored in 25 mM Tris-HCl at pH 8.0 and $I = 0.1$ (NaCl) containing 20% glycerol at −80 °C. The protein concentration was determined from the absorbance at 280 nm using extinction coefficients of 33,500 M^{-1} cm^{-1} for wildtype *c*TIM and 32,000 M^{-1} cm^{-1} for L7RM *c*TIM that were calculated using the ProtParam tool available on the Expasy server.[45,46]

The pET3a plasmid containing the gene coding for P168A mutant *Tbb*TIM was prepared in an earlier study.[41] P168A mutant *Tbb*TIM was overexpressed in *Escherichia Coli* BL21 pLys S grown in LB medium at 18 °C and purified by chromatography over a CM Sepharose column, as described previously.[47] Fractions that were judged to be homogeneous by gel electrophoresis were pooled, concentrated and stored at −80 °C in 25 mM TEA (pH 8.0) that contains 20% glycerol at $I = 0.15$ (NaCl). The protein concentration was determined from the absorbance at 280 nm using an extinction coefficient of 35,000 M^{-1} cm^{-1} calculated using the ProtParam tool available on the Expasy server.[45,46]

General Methods

Solution pH or pD was determined at 25 °C using an Orion model 720A pH meter equipped with a radiometer pHC4006-9 combination electrode that was standardized at pH 7.0 and 10.0. Values of pD were calculated by adding 0.40 to the observed reading of the pH meter.[48] Stock solutions of D,L-glyceraldehyde 3-phosphate (D,L-GAP) were prepared by hydrolysis of the corresponding diethyl acetal (barium salt) using Dowex 50WX4-200R (H^+ form) in boiling H_2O, as described previously.[14] The resulting solutions were stored at −20 °C and were adjusted to pH 7.5 by the addition of 1 M NaOH prior to use in enzyme assays. Stock solutions of buffers,[30,49] phosphite, [1-^{13}C]-glycolaldehyde ([1-^{13}C]-GA)[49] and 2-phosphoglycolate (PGA)[16] were prepared as described in previous work.

Enzyme Assays

All enzyme assays were carried out at pH 7.5, 25 °C and $I = 0.1$ (NaCl) according to procedures described in our previous work. α-Glycerol 3-phosphate dehydrogenase was assayed by monitoring the oxidation of NADH by DHAP,[14] and glyceraldehyde 3-phosphate dehydrogenase was assayed by monitoring the enzyme-catalyzed reduction of NAD^+ by GAP.[20] The TIM-catalyzed isomerization of GAP was monitored by coupling the formation of the product DHAP to the oxidation of NADH catalyzed by α-glycerol 3-phosphate dehydrogenase.[14,49] The TIM-catalyzed isomerization of DHAP was monitored by coupling the formation of the product GAP to the reduction of NAD^+ catalyzed by glyceraldehyde 3-phosphate dehydrogenase in the presence of 2 – 10 mM arsenate.[20,50]

Values of k_{cat} and K_m for TIM-catalyzed isomerization of GAP were determined from the nonlinear least squares fit of the initial velocity data to the Michaelis-Menten equation. Values of K_i for competitive inhibition of TIM by PGA at pH 7.5 ($I = 0.1$, NaCl) were determined by examining the effect of increasing concentrations of GAP on the initial velocity of TIM-catalyzed isomerization in the presence of two fixed concentrations of PGA. In these assays, the amount of the α-glycerol 3-phosphate dehydrogenase coupling enzyme was increased in order to overcome its inhibition by PGA. Values of k_{cat} and K_m for TIM-catalyzed isomerization of DHAP and the values of K_i for competitive inhibition by arsenate were determined by examining the effect of increasing concentrations of DHAP on the initial velocity of TIM-catalyzed isomerization in the presence of 2, 5, and 10 mM arsenate.

^{1}H NMR Analyses

^{1}H NMR spectra at 500 MHz were recorded in D_2O at 25 °C using a Varian Unity Inova 500 spectrometer that was shimmed to give a line width of ≤ 0.5 Hz for the most downfield peak of the double triplet due to the C-1 proton of the hydrate of [1-^{13}C]-GA.[49] Spectra (16 – 64 transients) were obtained using a sweep width of 6000 Hz, a pulse angle of 90° and an acquisition time of 6 s. A total relaxation delay of 120 s (> $8T_1$) between transients was used to ensure that accurate integrals were obtained for the protons of interest.[51,52] Baselines were subjected to a first-order drift correction before determination of integrated peak areas. Chemical shifts are reported relative to that for HOD at 4.67 ppm.

TIM-Catalyzed Reactions of [1-^{13}C]-GA in D_2O Monitored by ^{1}H NMR

The unactivated and phosphite dianion-activated reactions of [1-^{13}C]-GA catalyzed by wildtype *c*TIM, L7RM *c*TIM and P168A mutant *Tbb*TIM in D_2O at 25 °C were monitored by ^{1}H NMR spectroscopy, as described previously.[49] The enzymes were exhaustively dialyzed against 30 mM imidazole buffer (20% free base) in D_2O at pD 7.0 (I = 0.1, NaCl) for reactions in the absence of phosphite dianion, or against 30 mM imidazole buffer (20% free base) in D_2O at pD 7.0 (I = 0.024) for reactions in the presence of phosphite dianion. The unactivated TIM-catalyzed reactions of [1-^{13}C]-GA in the absence of phosphite dianion were initiated the addition of enzyme to give reaction mixtures (850 μL) containing 20 mM [1-^{13}C]-GA, 20 mM imidazole (20% free base) in D_2O at pD 7.0 and I = 0.1 and 0.34 mM wildtype *c*TIM, 0.48 mM L7RM *c*TIM or 0.22 – 0.49 mM P168A mutant *Tbb*TIM. The TIM-catalyzed reactions of [1-^{13}C]-GA in the presence of phosphite dianion were initiated by the addition of enzyme to give reaction mixtures (850 μL) containing 20 mM [1-^{13}C]-GA, 20 mM imidazole (20% free base), up to 20 mM HPO_3^{2-} (1:1 dianion:monoanion) in D_2O at pD 7.0 and I = 0.1 (NaCl) and 9 – 30 μM wildtype *c*TIM, 90 – 520 μM L7RM *c*TIM, or 60 – 350 μM P168A *Tbb*TIM. In each case, 750 μL of the reaction mixture was transferred to an NMR tube, the ^{1}H NMR spectrum was recorded immediately and spectra were then recorded at regular intervals. The remaining reaction mixture was incubated at 25 °C and was used to conduct periodic assays of the activity of TIM towards catalysis of isomerization of GAP. No significant loss in TIM activity was observed during any of these reactions which were followed for up to seven days. The reactions in the absence of phosphite dianion were followed until 70 – 80% completion and the reactions in the presence of phosphite dianion were typically followed until 40% completion, after which the protein was removed by ultrafiltration and the solution pD was determined. There was no significant change in pD during any of these reactions.

^{1}H NMR analyses the products of these reactions were conducted by monitoring the signals for the hydrates of the products [2-^{13}C]-GA, [2-^{13}C, 2-^{2}H]-GA, [1-^{13}C, 2-^{2}H]-GA and [1-^{13}C, 2,2-di-^{2}H]-GA and the fractional yields of these products, f_P, were determined at several times during the first 20 – 40% reaction, as described in our earlier work.[49] Observed first-order rate constants for the disappearance of [1-^{13}C]-GA, k_{obs} (s^{-1}), were determined from the slopes of linear semi-logarithmic plots of reaction progress against time covering the first 30 – 40% of the reaction, according to eq 1, where f_S is the fraction of [1-^{13}C]-GA remaining at time t. The observed second-order rate constants for the disappearance of [1-^{13}C]-GA, $(k_{cat}/K_m)_{obs}$ (M^{-1} s^{-1}), were calculated from the values of k_{obs} using eq 2, where f_{hyd} = 0.94 is the fraction of [1-^{13}C]-GA present in the unreactive hydrate form, and [E] is the concentration of TIM.[30]

$$\ln f_S = -k_{obs} t \quad (1)$$

$$(k_{\mathrm{cat}}/K_m)_{\mathrm{obs}}=\frac{k_{\mathrm{obs}}}{(1-f_{\mathrm{hyd}})[E]} \quad (2)$$

RESULTS

Kinetic Parameters and Inhibition Constants

Kinetic parameters k_{cat} and K_{m} for the isomerization of GAP catalyzed by wildtype *c*TIM, L7RM *c*TIM and P168A mutant *Tbb*TIM at pH 7.5, 25 °C and I = 0.1 (NaCl) were determined by Michaelis-Menten analyses of initial velocities and are reported in Table 1. Values of K_{i} for competitive inhibition of these TIMs by 2-phosphoglycolate (PGA) were determined from the dependence of the initial velocity of isomerization of GAP at several concentrations of GAP at two different fixed concentrations of PGA. These values of K_{i} (Table 1) were obtained from the nonlinear least squares fit of the initial velocity data to eq 3, where [I] = [PGA], and using the values of K_{m} given in Table 1. Arsenate is an activator of glyceraldehyde 3-phosphate dehydrogenase, which was used as the coupling enzyme in assays of the TIM-catalyzed isomerization of DHAP to give GAP.[20,50] The initial velocity of the isomerization of several concentrations of DHAP catalyzed by wildtype *c*TIM, L7RM *c*TIM and P168A mutant *Tbb*TIM at pH 7.5, 25 °C and I = 0.1 (NaCl) was determined in the presence of 2, 5 and 10 mM arsenate. Values of k_{cat} and K_{m} for the isomerization of DHAP, along with values of K_{i} for arsenate, were obtained from the nonlinear least squares fit of the initial velocity data to eq 3, where [I] = [arsenate], and are reported in Table 1.

$$\frac{v_i}{[E]}=\frac{k_{\mathrm{cat}}[\mathrm{GAP}]}{[\mathrm{GAP}]+K_m(1+[I]/K_i)} \quad (3)$$

TIM-Catalyzed Reactions of [1-^{13}C]-GA in D_2O

The disappearance of the substrate and the formation of the four identifiable products, shown in the boxes in Scheme 2, from the reaction of the truncated neutral substrate [1-^{13}C]-GA catalyzed by wildtype *c*TIM, L7RM *c*TIM and P168A *Tbb*TIM in D_2O buffered by 20 mM imidazole at pD 7.0, °C and I = 0.1 (NaCl) was monitored by ^{1}H NMR spectroscopy for up to seven days, as described previously.[20,49] The fractional yields of the products [2-^{13}C]-GA, [2-^{13}C, 2-^{2}H]-GA, [1-^{13}C, 2-^{2}H]-GA and [1-^{13}C, 2,2-di-^{2}H]-GA, f_{p}, were determined by ^{1}H NMR analysis at five different times during the disappearance of the first 20 - 40% of [1-^{13}C]-GA, as described in our previous work.[20,49] The observed first-order rate constants for the disappearance of [1-^{13}C]-GA in these reactions, k_{obs} (s^{-1}), were determined as the slopes of semi-logarithmic plots of reaction progress against time, according to eq 1. The observed second-order rate constants for the disappearance of [1-^{13}C]-GA, $(k_{\mathrm{cat}}/K_{\mathrm{m}})_{\mathrm{obs}}$ (M^{-1} s^{-1}), were calculated from the values of k_{obs} using eq 2.

Wildtype *c*TIM-Catalyzed Reactions of [1-^{13}C]-GA in D_2O

The relatively rapid phosphite-activated reactions of [1-^{13}C]-GA catalyzed by wildtype *c*TIM in D_2O in the presence of ≥ 2.0 mM HPO_3^{2-} result in essentially quantitative conversion of the substrate to the three products shown in Scheme 2A: [2-^{13}C]-GA, [2-^{13}C, 2-^{2}H]-GA and [1-^{13}C, 2-^{2}H]-GA (Table S1 of the Supporting Information).[49] By contrast, the very slow unactivated reaction of [1-^{13}C]-GA in the presence of wildtype *c*TIM gives the three products observed for the phosphite-activated reaction (Scheme 2A), along with a significant 19% yield of [1-^{13}C, 2,2-di-^{2}H]-GA that forms in a *nonspecific* protein-catalyzed reaction that occurs outside the active site of TIM (Scheme 2B), and the *total* yield of the

four identifiable products is only ca. 60% (Table S1 of the Supporting Information).[49] We proposed previously that [1-^{13}C, 2,2-di-^{2}H]-GA forms by a slow protein-catalyzed reaction that involves deuterium exchange into [1-^{13}C]-GA catalyzed by the amine side chains of surface lysine residues (Scheme 2B).[53] The absolute fractional yields of the products of the unactivated and phosphite dianion-activated wildtype *c*TIM-catalyzed reactions, f_P, are reported in Table S1 of the Supporting Information. There is good agreement between the fractional product yields from the phosphite dianion-activated reactions determined here and those reported earlier.[49] However, the *normalized* yields of 45% [2-^{13}C, 2-^{2}H]-GA and 42% [1-^{13}C, 2-^{2}H]-GA (Table S1 of the Supporting Information) from the *specific* reaction of [1-^{13}C]-GA at the active site of wildtype *c*TIM determined here are smaller and larger, respectively, than those of 60% and 30% reported earlier.[49] We conclude that, in our hands, the uncertainty in the yields of the products of the unactivated wildtype *c*TIM-catalyzed reactions of [1-^{13}C]-GA is larger than that for the phosphite dianion-activated reactions. These unactivated reactions of [1-^{13}C]-GA in the presence of TIM are very slow, were monitored for several days, and give only low yields of [2-^{13}C, 2-^{2}H]-GA and [1-^{13}C, 2-^{2}H]-GA (Table S1 of the Supporting Information). In addition, the signals of the multiplet due to the C-2 proton of [1-^{13}C, 2-^{2}H]-GA are not fully resolved from the very large doublet due to the C-2 proton of the substrate [1-^{13}C]-GA, which complicates the reliable determination of the yield of this product.[49]

Table S1 of the Supporting Information gives the *true* second-order rate constants k_{cat}/K_m (M^{-1} s^{-1}) for the wildtype *c*TIM-catalyzed reaction of the carbonyl form of [1-^{13}C]-GA to give the specific products of the TIM-catalyzed reaction [2-^{13}C]-GA, [2-^{13}C, 2-^{2}H]-GA and [1-^{13}C, 2-^{2}H]-GA (Scheme 2A). For the reactions in the presence of phosphite, these were calculated from the observed second-order rate constants $(k_{cat}/K_m)_{obs}$ using eq 4 with $\Sigma(f_P)_E = 1.0$, where $\Sigma(f_P)_E$ is the *sum* of the fractional yields of these specific products. A second-order rate constant of $k_{cat}/K_m = 0.1$ M^{-1} s^{-1} for the unactivated reaction in the absence of phosphite dianion was calculated using eq 4 with the values of $(k_{cat}/K_m)_{obs} = 0.19$ M^{-1} s^{-1} and $\Sigma(f_P)_E = 0.5$ reported in our previous work.[49]

$$\left(\frac{k_{\mathrm{cat}}}{K_m}\right)=\left(\frac{k_{\mathrm{cat}}}{K_m}\right)_{\mathrm{obs}}\sum\left(f_P\right)_E \quad (4)$$

Figure 1A shows the dependence of k_{cat}/K_m (M^{-1} s^{-1}) for the wildtype *c*TIM-catalyzed reactions of [1-^{13}C]-GA on the concentration of added phosphite dianion (HPO_3^{2-}).[30] The solid line shows the nonlinear least squares fit of these data to eq 5, derived for Scheme 3 (S = [1-^{13}C]-GA), with $(k_{cat}/K_m)_E = 0.1$ M^{-1} s^{-1} for the unactivated reaction in the absence of phosphite. The data give $(k_{cat}/K_m)_{E\bullet HPi} = 65$ M^{-1} s^{-1} for turnover of [1-^{13}C]-GA by the phosphite-liganded enzyme, and $K_d = 11$ mM for binding of phosphite dianion to the free enzyme (Table 3).[30] Table 3 also gives the corresponding kinetic parameters for the reactions of [1-^{13}C]-GA catalyzed by wildtype *Tbb*TIM that were determined in our earlier work.[54]

$$k_{\mathrm{cat}}/K_m=\left(\frac{K_d}{K_d+[\mathrm{HPO}_3^{2-}]}\right)\left(k_{\mathrm{cat}}/K_m\right)_E+\left(\frac{[\mathrm{HPO}_3^{2-}]}{K_d+[\mathrm{HPO}_3^{2-}]}\right)\left(k_{\mathrm{cat}}/K_m\right)_{E\bullet\mathrm{HPi}} \quad (5)$$

L7RM *c*TIM-Catalyzed Reactions of [1-^{13}C]-GA in D_2O

The 208-TGAG for 208-YGGS loop 7 replacement mutation of *c*TIM results in a decrease in the midpoint for thermal denaturation from 60 °C for the wildtype to 49 °C for L7RM cTIM.[28] However, despite this, we find that L7RM *c*TIM maintains full catalytic activity

over a period of seven days during the reaction of 20 mM [1-^{13}C]-GA at pD 7.0, 25 °C and I = 0.1 (NaCl).

Table S2 of the Supporting Information gives the fractional yields of the four identifiable products from the unactivated and phosphite dianion-activated L7RM *c*TIM-catalyzed reactions of [1-^{13}C]-GA that are shown in Scheme 2. The major product of the unactivated reaction of [1-^{13}C]-GA in the absence of phosphite dianion is [1-^{13}C, 2,2-di-^{2}H]-GA, which is formed in a yield of 27% by the nonspecific protein-catalyzed reaction shown in Scheme 2B. The very small yields of 1.5% [2-^{13}C, 2-^{2}H]-GA and ca. 0.2% [2-^{13}C]-GA show that L7RM *c*TIM maintains only a low activity for catalysis of the reactions of [1-^{13}C]-GA at the enzyme active site (Scheme 2A).[53] The observed yield of 3.3% [1-^{13}C, 2-^{2}H]-GA is formed by the both the specific reaction shown in Scheme 2A and the nonspecific reaction shown in Scheme 2B. A yield of ca. 1.1% [1-^{13}C, 2-^{2}H]-GA from only the specific reaction was estimated with the assumption that the *ratio* of the yields of [1-^{13}C, 2-^{2}H]-GA and [2-^{13}C, 2-^{2}H]-GA from the unactivated reaction is the same as that for the phosphite-activated reactions (see Table S2 of the Supporting Information).

Table 2 gives the *observed* second-order rate constants $(k_{cat}/K_m)_{obs}$ for the L7RM *c*TIM-catalyzed reactions of [1-^{13}C]-GA and the *true* second-order rate constants k_{cat}/K_m for the specific reactions at the active site of L7RM *c*TIM that were calculated from the values of $(k_{cat}/K_m)_{obs}$ using eq 4 with the values of $\Sigma(f_P)$ given in Table 2, where $\Sigma(f_P)_E$ is the *sum* of the fractional yields of these specific products (Table S2 of the Supporting Information).

Figure 1B shows the dependence of k_{cat}/K_m (M^{-1} s^{-1}) for the L7RM *c*TIM-catalyzed reactions of [1-^{13}C]-GA on the concentration of added phosphite dianion (HPO_3^{2-}).[30] The solid line shows the nonlinear least squares fit of these data to eq 5, with $(k_{cat}/K_m)_E$ = 0.0045 M^{-1} s^{-1} for the unactivated reaction in the absence of phosphite (Table 2). The data give $(k_{cat}/K_m)_{E\cdot HPi}$ = 0.39 M^{-1} s^{-1} for turnover of [1-^{13}C]-GA by the phosphite-liganded enzyme, and K_d = 4.1 mM for binding of phosphite dianion to the free enzyme (Table 3).[30] The upper limit for $(k_{cat}/K_m)_E$, calculated using eq 4 with the assumption that [1-^{13}C, 2-^{2}H]-GA forms exclusively by the specific pathway shown in Scheme 2A, is $(k_{cat}/K_m)_E \leq 0.008$ M^{-1} s^{-1}.

P168A *Tbb*TIM-Catalyzed Reactions of [1-^{13}C]-GA in D_2O

Table S3 of the Supporting Information gives the fractional yields of the four identifiable products from the unactivated and phosphite dianion-activated P168A *Tbb*TIM-catalyzed reactions of [1-^{13}C]-GA that are shown in Scheme 2. The major product of the unactivated reaction of [1-^{13}C]-GA in the absence of phosphite dianion is [1-^{13}C, 2,2-di-^{2}H]-GA, which is formed in a yield of 33% by the nonspecific protein-catalyzed pathway shown in Scheme 2B. There is only a small yield of 1.0% [2-^{13}C, 2-^{2}H]-GA and no detectable formation of [2-^{13}C]-GA. The observed yield of 11% [1-^{13}C, 2-^{2}H]-GA from both the specific reaction shown in Scheme 2A and the nonspecific reaction shown in Scheme 2B is substantially larger than the 3.3% yield of this product from the corresponding L7RM *c*TIM-catalyzed reaction, but similar to the 10% yield observed for the reaction catalyzed by a monomeric variant of *Tbb*TIM, for which there is no detectable activation by phosphite dianion.[54] These results are consistent with a relatively large activity of *Tbb*TIM for catalysis of deuterium exchange by the nonspecific pathway shown in Scheme 2B. *Tbb*TIM has an isoelectric point of 9.8,[55] which is 3 – 4 units higher than that for the TIMs from yeast,[55] and rabbit muscle.[55] We suggest that the greater reactivity of *Tbb*TIM in the pathway shown in Scheme 2B reflects a relatively large surface density of the amine side chains of lysine residues. A yield of ca. 1% [1-^{13}C, 2-^{2}H]-GA from only the specific reaction was estimated with the assumption that the *ratio* of the yields of [1-^{13}C, 2-^{2}H]-GA and [2-^{13}C, 2-^{2}H]-GA

from the unactivated reaction is the same as that for the phosphite-activated reactions (see Table S3 of the Supporting Information).

Table 2 gives the *observed* second-order rate constants $(k_{cat}/K_m)_{obs}$ for the P168A *Tbb*TIM-catalyzed reactions of [1-^{13}C]-GA and the *true* second-order rate constants k_{cat}/K_m for the specific reactions at the active site of P168A *Tbb*TIM that were calculated from the values of $(k_{cat}/K_m)_{obs}$ using eq 4 with the values of $\Sigma(f_P)$ given in Table 2, where $\Sigma(f_P)_E$ is the *sum* of the fractional yields of these specific products (Table S3 of the Supporting Information).

Figure 1C shows the dependence of k_{cat}/K_m (M^{-1} s^{-1}) for the P168A *Tbb*TIM-catalyzed reactions of [1-^{13}C]-GA on the concentration of added phosphite dianion (HPO_3^{2-}).[30] The solid line shows the nonlinear least squares fit of these data to eq 5, with $(k_{cat}/K_m)_E$ = 0.0013 M^{-1} s^{-1} for the unactivated reaction in the absence of phosphite (Table 2). The data give $(k_{cat}/K_m)_{E•HPi}$ = 0.83 M^{-1} s^{-1} for turnover of [1-^{13}C]-GA by the phosphite-liganded enzyme, and K_d = 10 mM for binding of phosphite dianion to the free enzyme (Table 3).[30] The upper limit for $(k_{cat}/K_m)_E$, calculated using eq 4 with the assumption that [1-^{13}C, 2-^{2}H]-GA forms exclusively by the specific pathway shown in Scheme 2A, is $(k_{cat}/K_m)_E \leq 0.008$ M^{-1} s^{-1}.

DISCUSSION

The TIMs from *Trypanosoma brucei brucei* (*Tbb*TIM) and chicken muscle (*c*TIM) exhibit 50% sequence indentity[56] and the active site structures determined for complexes of these two TIMs with phosphoglycolohydroxamate (PGH) are nearly superimposable.[54,57,58] No significant differences in the mechanism of action of TIM from these two sources have been observed,[59] and the mechanistic conclusions from studies on TIM from different organisms have been broadly generalized to all TIMs, except perhaps the enzymes from archaea.[28,29] The kinetic parameters for wildtype and mutant TIMs determined here (Table 1) are in agreement with those reported earlier.[28,41,60] The P168A mutation of *Tbb*TIM and the loop 7 replacement mutation of *c*TIM result in 30- and 190-fold decreases, respectively, in k_{cat}/K_m for catalysis of isomerization of GAP, which are due largely to the effects of these mutations on k_{cat} (Table 1). The loop 7 replacement mutant of *c*TIM results in a 120-fold increase in K_i for competitive inhibition by 2-phosphoglycolate (PGA) at pH 7.5. PGA is an early example of a tight-binding enzyme inhibitor that was proposed to be an analog of the enediolate-like transition state for the catalyzed reaction (Chart 1).[61–63] The observation that the loop 7 replacement mutation results in similar large changes in k_{cat}/K_m for isomerization of GAP and DHAP and in K_i for inhibition by PGA shows that this mutation weakens, to a similar extent, interactions that stabilize the TIM•PGA complex and the transition state for isomerization. By contrast, the P168A mutation of *Tbb*TIM results in only a 2-fold increase in K_i for inhibition by PGA, which is significantly smaller than the 30-fold effect of this mutation on k_{cat}/K_m for the *Tbb*TIM-catalyzed isomerization of GAP. This shows that the P168A mutation affects interactions that control the barrier for formation of the enzyme-bound transition state, but which do not strongly stabilize the TIM•PGA complex.

Reactions of Substrate Pieces

We have characterized the activation of wildtype and mutant TIM-catalyzed reactions of the truncated neutral substrate glycolaldehyde (GA) by phosphite dianion in terms of three kinetic parameters (Scheme 4). (1) The second-order rate constant $(k_{cat}/K_m)_E$ for the unactivated reaction catalyzed by the free enzyme in the absence of phosphite. (2) The second-order rate constant $(k_{cat}/K_m)_{E•HPi}$ for the reaction catalyzed by the binary $E•HPO_3^{2-}$ complex. (3) The disassociation constant K_d for breakdown of the $E•HPO_3^{2-}$ complex, which measures the affinity of the free enzyme for phosphite dianion. Additionally, the dissociation constant for release of phosphite from the *transition state,* $K_d^{‡}$ (Scheme 4),

which is a measure of the intrinsic phosphite binding energy, may then be calculated from these three experimental parameters according to eq 6. Table 3 summarizes these parameters for the wildtype and mutant TIM studied here, along with the *third-order* rate constants ($k_{cat}/K_m)_{E•HPi}/K_d$ (M^{-2} s^{-1}) for the reactions of the two-part substrate GA + phosphite.

$$K_d^{\ddagger}=\frac{K_d(k_{\rm cat}/K_m)_E}{(k_{\rm cat}/K_m)_{E\bullet{\rm HPi}}} \quad (6)$$

The P168A mutation of *Tbb*TIM results in similar 30- and 40-fold decreases, respectively, in the second-order rate constant k_{cat}/K_m (Table 1) for the reaction of the whole substrate GAP and the third-order rate constant $(k_{cat}/K_m)_{E•HPi}/K_d$ (Table 3) for reaction of the substrate pieces GA + phosphite, while the loop 7 replacement mutation of *c*TIM results in a slightly larger 190-decrease in k_{cat}/K_m for GAP and a 60-fold decrease in $(k_{cat}/K_m)_{E•HPi}/K_d$ for the pieces. We conclude that these quite different structural mutations result in a similar loss of stabilizing interactions between the protein and the transition state for the enzyme-catalyzed reaction of both the whole substrate GAP and the substrate pieces GA + HPO_3^{2-}. These results add to a large body of data that are consistent with the conclusion that the primary effect of covalent connections between substrate pieces,[20,30–32,34,64–66] or in some cases enzyme pieces,[17,67] is to reduce the unfavorable entropic barrier associated with the reaction of the pieces, relative to that for the reaction of whole substrate or enzyme.[68]

The well-documented phosphodianion-driven conformational change of TIM has been incorporated into the model shown in Scheme 5, which rationalizes the activation of the enzyme by the binding of HPO_3^{2-}.[20,21,49] In this model, TIM exists in a dominant loop open enzyme form $\mathbf{E_O}$ that is inactive, and a rare, higher energy but active, loop-closed enzyme form $\mathbf{E_C}$ ($K_c \ll 1$, Scheme 5). A large fraction of the free energy barrier for the conversion of $\mathbf{E_O}$ to $\mathbf{E_C}$ may represent the barrier to desolvation of the enzyme active site that accompanies ligand binding and loop closure.[18,37] The loop-closed form shows specificity for binding of both HPO_3^{2-} and the transition state for the reaction of the substrate piece, $GA^{\ddagger}$. The overall binding affinity of HPO_3^{2-} and of the transition state $GA^{\ddagger}$ to free TIM is relatively weak, because a substantial portion of the ligand binding energy is used to drive the transformation from inactive $\mathbf{E_O}$ to active $\mathbf{E_C}$ in forming the binary $\mathbf{E_C}$•HPO_3^{2-} or $\mathbf{E_C}$•$GA^{\ddagger}$ complexes (Scheme 5). By contrast, the full intrinsic binding energy of the second ligand is observed upon conversion of these binary complexes of the ternary $\mathbf{E_C}$•HPO_3^{2-}•$GA^{\ddagger}$ complex. We use Scheme 5 as the framework for our discussion of structure-reactivity relationships for the P168A and loop 7 replacement mutations of TIM.

P168A Mutation

Figure 2 shows the X-ray crystal structures in the active site region of unliganded wildtype *Tbb*TIM (gold, 2.1 Å resolution),[69] PGA-liganded wildtype TIM from *Leishmania mexicana* (cyan, 0.83 Å resolution),[70] and PGA-liganded P168A mutant *Tbb*TIM (green, 1.15 Å resolution).[41] A comparison of the X-ray crystal structures for unliganded wildtype and P168A mutant *Tbb*TIM shows that the mutation causes only small changes in protein structure.[41] The binding of PGA to wildtype TIM (Figure 2, gold) triggers the large conformational change to give the loop-closed enzyme (Figure 2, green).[41] This movement of loop 6 from the open to the closed conformation is accompanied by 90° and 180° rotations, respectively, in the planes defined by the peptide bonds of Gly211 and Gly212, which results in a steric clash between the carbonyl oxygen of Gly211 and the pyrolidine side chain of Pro168.[71] This strain is relieved by movement of the pyrolidine ring of Pro168 that “swings” the neighboring carboxylate side chain of the active site base Glu167 toward the PGA ligand.[41,71] Figure 2 shows that the binding of PGA to the P168A mutant of

*Tbb*TIM triggers nearly the same conformational change as that observed for wildtype TIM. However, the effect of replacement of the cyclic pyrolidine side chain with the smaller methyl group at position 168 is to remove the steric clash with the mobile carbonyl oxygen of Gly211, so that the side chain of Glu167 remains in the "swung out" position that is observed for *unliganded open* wildtype TIM.[41] PGA binds, formally, as the trianion to TIM and this binding is accompanied by the uptake of a proton by Glu167 that results in the formation of a hydrogen bond between the carboxyl groups of bound PGA and Glu167.[19] The P168A mutation of *Tbb*TIM results in movement of the PGA ligand toward the nearly stationary side chain of Glu167. This preserves the ligand-side chain hydrogen bond (Figure 2), and so may provide a rationalization for the small effect of the mutation on K_i for inhibition by PGA (Table 1).

Figures 3A and 3B show free energy diagrams, constructed for the model shown in Scheme 5, illustrating the effect of the P168A mutation of *Tbb*TIM on the unactivated and phosphite-activated TIM-catalyzed reactions of GA. The free energies of activation were calculated from the kinetic parameters given in Table 3 using the Eyring equation at 298 K, and with the assumption that the phosphite dianion functions solely as a "spectator" to hold TIM in the active closed E_C form, so that $(k_{cat}/K_m)_E' = (k_{cat}/K_m)_{E\bullet HPi}$ (Scheme 5).[20,30] The free energy barrier to the unactivated wildtype enzyme-catalyzed reaction of GA, calculated from $(k_{cat}/K_m)_E$, can be partitioned into the barrier for the conformational change that converts the inactive enzyme E_O to the active enzyme E_C (given by $-RT\ln K_C$, eq 7), and the barrier to catalysis by the active closed enzyme $(k_{cat}/K_m)_E' = (k_{cat}/K_m)_{E\bullet HPi}$ (Scheme 5).

$$\left(\frac{1}{K_C}\right) = \frac{(k_{cat}/K_m)_{E\bullet HPi}}{(k_{cat}/K_m)_E} \quad (7)$$

The carboxylate anion side chain of Glu167 at the P168A mutant enzyme-PGA complex remains in the "swung out" position, compared with the "swung in" position for wildtype *Tbb*TIM (Figure 2). This structural change results in a 30-fold fold decrease in k_{cat}/K_m for enzyme-catalyzed isomerization of GAP (Table 1), and 50-fold and 80-fold decreases, respectively, in $(k_{cat}/K_m)_E$ and $(k_{cat}/K_m)_{E\bullet HPi}$ for deprotonation of GA by TIM and by the TIM•HPO_3^{2-} complex (Table 3). There is also almost no effect of the P168A mutation on the ratio of the second-order rate constants for the reactions of GA catalyzed by the free enzyme and the phosphite-liganded enzyme, $(k_{cat}/K_m)_{E\bullet HPi}/(k_{cat}/K_m)_E$. This is consistent with only a small effect of this mutation on the equilibrium constant for interconversion of the open inactive and closed active forms of the enzyme, K_C (eq 7), so that the change in $(k_{cat}/K_m)_E$ is due mainly to the change in $(k_{cat}/K_m)_E' \approx (k_{cat}/K_m)_{E\bullet HPi}$. Finally, there is almost no effect of the mutation on $K_d^{\ddagger}$ for binding of phosphite dianion to the transition state $\mathbf{E_C}$•GA‡ (Table 3), resulting in essentially identical intrinsic phosphite dianion binding energies of 6.4 and 6.5 kcal/mol, respectively for the wildtype and P168A mutant *Tbb*TIM (Figure 3).

The decreases in $(k_{cat}/K_m)_E$ and $(k_{cat}/K_m)_{E\bullet HPi}$ observed for P168A mutant *Tbb*TIM reflect the increases in the reaction barrier associated with the shift in the side chain of Glu167 away from its optimally aligned "swung in" position at the wildtype enzyme.[72] The P168A mutation is not expected to alter protein-phosphodianion interactions and we observe no effect of this mutation on the intrinsic phosphite binding energy (Figure 3). Calculations are consistent with the conclusion that the 5-membered pyrolidine ring of the side chain of Pro168 adopts a strained planar configuration at the complex between PGA and TIM from *Leishmania mexicana*.[70,73] The relief of this strain by excision of the pyrolidine ring at the P168A mutant would be expected to stabilize the active enzyme $\mathbf{E_C}$ relative to the inactive enzyme $\mathbf{E_O}$ and result in an increase in K_C. However, our results can be rationalized by only

a small effect of the mutation on K_C, as discussed above. The small effect of the P168A mutation on the relative barriers to $(k_{cat}/K_m)_E$ and $(k_{cat}/K_m)_{E•HPi}$ might reflect a compensating increase in K_C and decrease in $(k_{cat}/K_m)_E'$, but we can provide no simple rationalization for such compensating changes.

Loop 7 Replacement Mutation

The binding of the enediolate intermediate analog PGH to *c*TIM results in the formation of a stunning array of hydrogen bonding interactions with loop 7 (Figure 4).[27] These include (1) Inter-loop H-bonds between: (a) the backbone amide NH of Gly173 from loop 6 and the γ-O of Ser-211 from loop 7; (b) the backbone amide NH of Ala-176 from loop 6 and the phenol oxygen of Try208 from loop 7; and (c) the carbonyl oxygen of Ala169 from loop 6 and the γ-OH of Ser211 from loop 7. (2) Hydrogen bonds between the phosphodianion group of PGH and the backbone amide NH groups of Ser-211.[58] This hydrogen bonding pattern has been perturbed by substitution of the YGGS motif at residues 208 – 211 with 208-TGAG sequence commonly found at archaeal organisms.[28] Like the P168A mutation, this structural mutation results in significant decreases in $(k_{cat}/K_m)_{E•HPi}$ and $(k_{cat}/K_m)_E$. Inspection of Figure 4 suggests that the L7RM should have no effect on the important protein-phosphodianion interactions, so that no change in the intrinsic phosphite dianion binding energy is expected, and only a small 2.5-fold increase in $K_d^‡$ is observed (Table 3).

The values of $(k_{cat}/K_m)_{E•HPi}$ and $(k_{cat}/K_m)_E$ for L7RM *c*TIM are 2-fold smaller and 3-fold larger respectively than the corresponding kinetic parameters for P168A mutant *Tbb*TIM (Table 3). This difference reflects the similar effects of the P168A mutation on $(k_{cat}/K_m)_{E•HPi}$ and $(k_{cat}/K_m)_E$ discussed above, compared with the larger decrease in $(k_{cat}/K_m)_{E•HPi}$ relative to $(k_{cat}/K_m)_E$ determined for the L7RM of *c*TIM. We propose that the P168A mutation has little effect on the magnitude of phosphite dianion activation of TIM-catalyzed reactions of GA, while the loop 7 replacement mutation results in a significant reduction in dianion activation. These results are consistent with a 6.5-fold decrease in the value of $1/K_C$ (eq 7), from 650 for wildtype *c*TIM to 100 for L7RM *c*TIM (Table 3).

Mechanism for Dianion Activation

The primary imperative for models for enzyme activation by HPO_3^{2-} is to provide a rationalization for the specificity of phosphite dianion in binding to the transition state complex E•GA‡ ($K_d^‡$, Scheme 4). The specificity of the closed enzyme $\mathbf{E_C}$ for binding both GA‡ and HPO_3^{2-} (Scheme 5) provides for the tighter binding of HPO_3^{2-} to the transition state complex E•GA‡ compared with free enzyme that exists mainly as $\mathbf{E_O}$ (Figure 3). Selectivity in the binding of HPO_3^{2-} to the E•GA‡ transition state complex might be the result of a direct stabilizing interaction between GA‡ and phosphite dianion. We discount this possibility for the following reasons. First, the electrostatic interaction between phosphite dianion and the enolate-anion like transition state for deprotonation of carbon is destabilizing. Second, only weak stabilizing intermolecular Van der Waals interactions are expected for these small polar molecules. Third, only a single intermolecular hydrogen bond between the C-2 hydroxyl of GA and phosphite dianion is possible. However, inspection of X-ray crystal structures shows that the ligands adopt an extended conformation when bound to TIM (for example, see Figure 2). A stabilizing intermolecular hydrogen bond is unlikely to form at a transition state ternary complex E•GA•HPO_3^{2-} that adopts a similar conformation.

The P168A and the loop 7 replacement mutations of TIM result in an increase in the activation barriers to TIM-catalyzed deprotonation of GA, but little change in the intrinsic phosphite dianion binding energy. This result is consistent with a catalytic site at TIM that operates independently from the dianion activation site. The catalytic and activating sites

must interact to the extent that dianion binding at the activator site triggers a conformational change that extends to the catalytic site. We propose for TIM (Scheme 5) that GA and HPO_3^{2-} bind essentially independently at the protein and that: (a) The binding of HPO_3^{2-} at the dianion site plays the passive role of stabilizing the preexisting active enzyme $\mathbf{E_C}$, but does not affect the structure or intrinsic catalytic activity of $\mathbf{E_C}$. (b) The binding of GA to $\mathbf{E_C}$ has little or no effect on the affinity of HPO_3^{2-} at the catalytic site. The result of the independent binding of the substrate pieces is to sequester GA at the catalytically active closed form of TIM. The binding loci for GA and HPO_3^{2-} lie essentially adjacent to one another at the active site for TIM, so that some structural mutations may affect the enzyme structure and function at both sites.

Finally, we note that mutations that affect the relative stability of $\mathbf{E_C}$ and $\mathbf{E_O}$ (K_C, Scheme 5) may show complex effects on the kinetic parameters for catalysis of substrate deprotonation, and on the magnitude of enzyme activation by phosphite dianion, as has been discussed in an earlier study of the L232A mutation of *Tbb*TIM.[20,21] The data reported in this paper are consistent with a small 6.5-fold effect of the L7RM on K_C that is reflected by the 6.5 fold decrease in the magnitude of the enzyme activation by phosphite dianion (Table 3).

Supplementary Material

Refer to Web version on PubMed Central for supplementary material.

ABBREVIATIONS

TIM	triosephosphate isomerase
***Tbb*TIM**	TIM from *Trypanosoma brucei brucei*
***c*TIM**	TIM from chicken muscle
DHAP	dihydroxyacetone phosphate
GAP	(*R*)-glyceraldehyde 3-phosphate
GA	glycolaldehyde
PGA	2-phosphoglycolate
PGH	phosphoglycolohydroxamate
L7RM	loop 7 replacement mutant
NADH	nicotinamide adenine dinucleotide, reduced form
NAD^+	nicotinamide adenine dinucleotide, oxidized form
NMR	nuclear magnetic resonance,

References

1. Knowles JR, Albery WJ. Perfection in enzyme catalysis: the energetics of triosephosphate isomerase. Acc Chem Res. 1977; 10:105–111.
2. Knowles JR. To build an enzyme. Philos Trans R Soc London, Ser B. 1991; 332:115–121. [PubMed: 1678530]
3. Coulson AFW, Knowles JR, Priddle JD, Offord RE. Uniquely labeled active site sequence in chicken muscle triose phosphate isomerase. Nature (London). 1970; 227:180–181. [PubMed: 5428407]

4. Hartman FC. Isolation and characterization of an active-site peptide from triose phosphate isomerase. J Am Chem Soc. 1970; 92:2170–2172. [PubMed: 5461608]
5. Waley SG, Miller JC, Rose IA, O'Connell EL. Identification of site in triose phosphate isomerase labeled by glycidol phosphate. Nature (London). 1970; 227:181. [PubMed: 5428408]
6. Joseph-McCarthy D, Rost LE, Komives EA, Petsko GA. Crystal Structure of the Mutant Yeast Triosephosphate Isomerase in Which the Catalytic Base Glutamic Acid 165 Is Changed to Aspartic Acid. Biochemistry. 1994; 33:2824–2829. [PubMed: 7907502]
7. Lodi PJ, Knowles JR. Neutral imidazole is the electrophile in the reaction catalyzed by triosephosphate isomerase: structural origins and catalytic implications. Biochemistry. 1991; 30:6948–6956. [PubMed: 2069953]
8. Komives EA, Chang LC, Lolis E, Tilton RF, Petsko GA, Knowles JR. Electrophilic catalysis in triosephosphate isomerase: the role of histidine-95. Biochemistry. 1991; 30:3011–3019. [PubMed: 2007138]
9. Nickbarg EB, Davenport RC, Petsko GA, Knowles JR. Triosephosphate isomerase: removal of a putatively electrophilic histidine residue results in a subtle change in catalytic mechanism. Biochemistry. 1988; 27:5948–5960. [PubMed: 2847777]
10. Gerlt JA, Gassman PG. An Explanation for Rapid Enzyme-Catalyzed Proton Abstraction from Carbon Acids: Importance of Late Transition States in Concerted Mechanisms. J Am Chem Soc. 1993; 115:11552–11568.
11. Richard JP, Amyes TL. Proton transfer at carbon. Curr Opin Chem Biol. 2001; 5:626–633. [PubMed: 11738171]
12. Rieder SV, Rose IA. Mechanism of the triose phosphate isomerase reaction. J Biol Chem. 1959; 234:1007–1010. [PubMed: 13654309]
13. O'Donoghue AC, Amyes TL, Richard JP. Hydron Transfer Catalyzed by Triosephosphate Isomerase. Products of Isomerization of Dihydroxyacetone Phosphate in D_2O. Biochemistry. 2005; 44:2622–2631. [PubMed: 15709775]
14. O'Donoghue AC, Amyes TL, Richard JP. Hydron Transfer Catalyzed by Triosephosphate Isomerase. Products of Isomerization of (R)-Glyceraldehyde 3-Phosphate in D_2O. Biochemistry. 2005; 44:2610–2621. [PubMed: 15709774]
15. Knowles JR. Enzyme catalysis: not different, just better. Nature. 1991; 350:121–124. [PubMed: 2005961]
16. Go MK, Koudelka A, Amyes TL, Richard JP. Role of Lys-12 in Catalysis by Triosephosphate Isomerase: A Two-Part Substrate Approach. Biochemistry. 2010; 49:5377–5389. [PubMed: 20481463]
17. Go MK, Amyes TL, Richard JP. Rescue of K12G Triosephosphate Isomerase by Ammonium Cations: The Reaction of an Enzyme in Pieces. J Am Chem Soc. 2010; 132:13525–13532. [PubMed: 20822141]
18. Richard JP. A Paradigm for Enzyme-Catalyzed Proton Transfer at Carbon: Triosephosphate Isomerase. Biochemistry. 2012; 51:2652–2661. [PubMed: 22409228]
19. Malabanan MM, Nitsch-Velasquez L, Amyes TL, Richard JP. Magnitude and Origin of the Enhanced Basicity of the Catalytic Glutamate of Triosephosphate Isomerase. J Am Chem Soc. 2013; 135:5978–5981. [PubMed: 23560625]
20. Malabanan MM, Koudelka AP, Amyes TL, Richard JP. Mechanism for Activation of Triosephosphate Isomerase by Phosphite Dianion: The Role of a Hydrophobic Clamp. J Am Chem Soc. 2012; 134:10286–10298. [PubMed: 22583393]
21. Malabanan MM, Amyes TL, Richard JP. Mechanism for Activation of Triosephosphate Isomerase by Phosphite Dianion: The Role of a Ligand-Driven Conformational Change. J Am Chem Soc. 2011; 133:16428–16431. [PubMed: 21939233]
22. Pompliano DL, Peyman A, Knowles JR. Stabilization of a reaction intermediate as a catalytic device: definition of the functional role of the flexible loop in triosephosphate isomerase. Biochemistry. 1990; 29:3186–3194. [PubMed: 2185832]
23. Sampson NS, Knowles JR. Segmental movement: definition of the structural requirements for loop closure in catalysis by triosephosphate isomerase. Biochemistry. 1992; 31:8482–8487. [PubMed: 1390632]

24. Sampson NS, Knowles JR. Segmental motion in catalysis: investigation of a hydrogen bond critical for loop closure in the reaction of triosephosphate isomerase. Biochemistry. 1992; 31:8488–8494. [PubMed: 1390633]
25. Xiang J, Jung J-y, Sampson NS. Entropy effects on protein hinges: The reaction catalyzed by triosephosphate isomerase. Biochemistry. 2004; 43:11436–11445. [PubMed: 15350130]
26. Xiang J, Sun J, Sampson NS. The importance of hinge sequence for loop function and catalytic activity in the reaction catalyzed by triosephosphate isomerase. J Mol Biol. 2001; 307:1103–1112. [PubMed: 11286559]
27. Malabanan MM, Amyes Tina L, Richard John P. A role for flexible loops in enzyme catalysis. Cur Opin Struct Biol. 2010; 20:702–710.
28. Wang Y, Berlow RB, Loria JP. Role of Loop-Loop Interactions in Coordinating Motions and Enzymatic Function in Triosephosphate Isomerase. Biochemistry. 2009; 48:4548–4556. [PubMed: 19348462]
29. Kursula I, Salin M, Sun J, Norledge BV, Haapalainen AM, Sampson NS, Wierenga RK. Understanding protein lids: structural analysis of active hinge mutants in triosephosphate isomerase. Prot Eng, Des & Sel. 2004; 17:375–382.
30. Amyes TL, Richard JP. Enzymatic Catalysis of Proton Transfer at Carbon: Activation of Triosephosphate Isomerase by Phosphite Dianion. Biochemistry. 2007; 46:5841–5854. [PubMed: 17444661]
31. Amyes TL, Richard JP, Tait JJ. Activation of orotidine 5′-monophosphate decarboxylase by phosphite dianion: The whole substrate is the sum of two parts. J Am Chem Soc. 2005; 127:15708–15709. [PubMed: 16277505]
32. Goryanova B, Amyes TL, Gerlt JA, Richard JP. OMP Decarboxylase: Phosphodianion Binding Energy Is Used To Stabilize a Vinyl Carbanion Intermediate. J Am Chem Soc. 2011; 133:6545–6548. [PubMed: 21486036]
33. Amyes TL, Wood BM, Chan K, Gerlt JA, Richard JP. Formation and Stability of a Vinyl Carbanion at the Active Site of Orotidine 5′-Monophosphate Decarboxylase: pK_a of the C-6 Proton of Enzyme-Bound UMP. J Am Chem Soc. 2008; 130:1574–1575. [PubMed: 18186641]
34. Tsang WY, Amyes TL, Richard JP. A Substrate in Pieces: Allosteric Activation of Glycerol 3-Phosphate Dehydrogenase (NAD^+) by Phosphite Dianion. Biochemistry. 2008; 47:4575–4582. [PubMed: 18376850]
35. Ray WJ Jr, Long JW, Owens JD. An analysis of the substrate-induced rate effect in the phosphoglucomutase system. Biochemistry. 1976; 15:4006–4017. [PubMed: 963019]
36. Kholodar SA, Murkin AS. DXP Reductoisomerase: Reaction of the Substrate in Pieces Reveals a Catalytic Role for the Nonreacting Phosphodianion Group. Biochemistry. 2013; 52:2302–2308. [PubMed: 23473304]
37. Amyes TL, Richard JP. Specificity in Transition State Binding: The Pauling Model Revisited. Biochemistry. 2013; 52:2021–2035.
38. Jencks WP. Binding Energy, Specificity and Enzymic Catalysis: The Circe Effect. Adv Enzymology Relat Areas Mol Biol. 1975; 43:219–410.
39. Wang C, Rance M, Palmer AG. Mapping Chemical Exchange in Proteins with MW > 50 kD. J Am Chem Soc. 2003; 125:8968–8969. [PubMed: 15369325]
40. Igumenova TI, Palmer AG. Off-Resonance TROSY-Selected R1ρ Experiment with Improved Sensitivity for Medium- and High-Molecular-Weight Proteins. J Am Chem Soc. 2006; 128:8110–8111. [PubMed: 16787055]
41. Casteleijn MG, Alahuhta M, Groebel K, El-Sayed I, Augustyns K, Lambeir AM, Neubauer P, Wierenga RK. Functional role of the conserved active site proline of triosephosphate isomerase. Biochemistry. 2006; 45:15483–15494. [PubMed: 17176070]
42. O'Connor EJ, Tomita Y, McDermott AE. Synthesis of (1,2-C-$^{13}C_2$) 2-Phosphoglycolic acid. J Lab Comp & Radio. 1994; 34:735–740.
43. Desai KK, Miller BG. A Metabolic Bypass of the Triosephosphate Isomerase Reaction. Biochemistry. 2008; 47:7983–7985. [PubMed: 18620424]
44. Sun J, Sampson NS. Understanding Protein Lids: Kinetic Analysis of Active Hinge Mutants in Triosephosphate Isomerase. Biochemistry. 1999; 38:11474–11481. [PubMed: 10471299]

45. Gasteiger E, Hoogland C, Gattiker A, Duvaud S, Wilkins MR, Appel RD, Bairoch A. Protein identification and analysis tools on the ExPASy server. Proteomics Protoc Handb. 2005:571–607.
46. Gasteiger E, Gattiker A, Hoogland C, Ivanyi I, Appel RD, Bairoch A. ExPASy: the proteomics server for in-depth protein knowledge and analysis. Nucleic Acids Res. 2003; 31:3784–3788. [PubMed: 12824418]
47. Borchert TV, Pratt K, Zeelen JP, Callens M, Noble MEM, Opperdoes FR, Michels PAM, Wierenga RK. Overexpression of trypanosomal triosephosphate isomerase in Escherichia coli and characterization of a dimer-interface mutant. Eur J Biochem. 1993; 211:703–710. [PubMed: 8436128]
48. Glasoe PK, Long FA. Use of glass electrodes to measure acidities in deuterium oxide. J Phys Chem. 1960; 64:188–190.
49. Go MK, Amyes TL, Richard JP. Hydron Transfer Catalyzed by Triosephosphate Isomerase. Products of the Direct and Phosphite-Activated Isomerization of [1-^{13}C]-Glycolaldehyde in D_2O. Biochemistry. 2009; 48:5769–5778. [PubMed: 19425580]
50. Plaut B, Knowles JR. pH-Dependence of the triose phosphate isomerase reaction. Biochem J. 1972; 129:311–320. [PubMed: 4643319]
51. Amyes TL, Richard JP. Determination of the pK_a of Ethyl Acetate: Brønsted Correlation for Deprotonation of a Simple Oxygen Ester in Aqueous Solution. J Am Chem Soc. 1996; 118:3129–3141.
52. Amyes TL, Richard JP. Generation and stability of a simple thiol ester enolate in aqueous solution. J Am Chem Soc. 1992; 114:10297–10302.
53. Go MK, Malabanan MM, Amyes TL, Richard JP. Bovine Serum Albumin-Catalyzed Deprotonation of [1-^{13}C]-Glycolaldehyde: Protein Reactivity toward Deprotonation of α-Hydroxy α-Carbonyl Carbon. Biochemistry. 2010; 49:7704–7708. [PubMed: 20687575]
54. Malabanan MM, Go MK, Amyes TL, Richard JP. Wildtype and engineered monomeric triosephosphate isomerase from Trypanosoma brucei: Partitioning of reaction intermediates in D_2O and activation by phosphite dianion. Biochemistry. 2011; 50:5767–5779. [PubMed: 21553855]
55. Misset O, Bos OJ, Opperdoes FR. Glycolytic enzymes of Trypanosoma brucei. Simultaneous purification, intraglycosomal concentrations and physical properties. Eur J Biochem. 1986; 157:441–453. [PubMed: 2940090]
56. Wierenga RK, Noble MEM, Davenport RC. Comparison of the refined crystal structures of liganded and unliganded chicken, yeast and trypanosomal triosephosphate isomerase. J Mol Biol. 1992; 224:1115–1126. [PubMed: 1569570]
57. Alahuhta M, Wierenga RK. Atomic resolution crystallography of a complex of triosephosphate isomerase with a reaction-intermediate analog: New insight in the proton transfer reaction mechanism. Proteins Struct, Funct, Bioinf. 2010; 78:1878–1888.
58. Zhang Z, Sugio S, Komives EA, Liu KD, Knowles JR, Petsko GA, Ringe D. Crystal Structure of Recombinant Chicken Triosephosphate Isomerase-Phosphoglycolohydroxamate Complex at 1.8-Å Resolution. Biochemistry. 1994; 33:2830–2837. [PubMed: 8130195]
59. Wierenga RK, Kapetaniou EG, Venkatesan R. Triosephosphate isomerase: a highly evolved biocatalyst. Cell Mol Life Sci. 2010; 67:3961–3982. [PubMed: 20694739]
60. Putman SJ, Coulson AFW, Farley IRT, Riddleston B, Knowles JR. Specificity and kinetics of triose phosphate isomerase from chicken muscle. Biochem J. 1972; 129:301–310. [PubMed: 4643318]
61. Hartman FC, LaMuraglia GM, Tomozawa Y, Wolfenden R. The influence of pH on the interaction of inhibitors with triosephosphate isomerase and determination of the pK_a of the active-site carboxyl group. Biochemistry. 1975; 14:5274–5279. [PubMed: 47]
62. Wolfenden R. Analog approaches to the structure of the transition state in enzyme reactions. Acc Chem Res. 1972; 5:10–18.
63. Wolfenden R. Transition state analogues for enzyme catalysis. Nature. 1969; 223:704–705. [PubMed: 4979456]

64. Goryanova B, Spong K, Amyes TL, Richard JP. Catalysis by Orotidine 5′-Monophosphate Decarboxylase: Effect of 5-Fluoro and 4′-Substituents on the Decarboxylation of Two-Part Substrates. Biochemistry. 2013; 52:537–546. [PubMed: 23276261]

65. Amyes TL, Ming SA, Goldman LM, Wood BM, Desai BJ, Gerlt JA, Richard JP. Orotidine 5′-monophosphate decarboxylase: Transition state stabilization from remote protein-phosphodianion interactions. Biochemistry. 2012; 51:4630–4632. [PubMed: 22620855]

66. Barnett SA, Amyes TL, Wood BM, Gerlt JA, Richard JP. Dissecting the Total Transition State Stabilization Provided by Amino Acid Side Chains at Orotidine 5′-Monophosphate Decarboxylase: A Two-Part Substrate Approach. Biochemistry. 2008; 47:7785–7787. [PubMed: 18598058]

67. Barnett SA, Amyes TL, McKay WB, Gerlt JA, Richard JP. Activation of R235A Mutant Orotidine 5′-Monophosphate Decarboxylase by the Guanidinium Cation: Effective Molarity of the Cationic Side Chain of Arg-235. Biochemistry. 2010; 49:824–826. [PubMed: 20050635]

68. Jencks WP. On the attribution and additivity of binding energies. Proc Natl Acad Sci, USA. 1981; 78:4046–4050. [PubMed: 16593049]

69. Noble ME, Zeelen JP, Wierenga RK. Structures of the “open” and “closed” state of trypanosomal triosephosphate isomerase, as observed in a new crystal form: implications for the reaction mechanism. Proteins. 1993; 16:311–326. [PubMed: 8356028]

70. Kursula I, Wierenga RK. Crystal structure of triosephosphate isomerase complexed with 2-phosphoglycolate at 0.83 Å resolution. J Biol Chem. 2003; 278:9544–9551. [PubMed: 12522213]

71. Noble ME, Zeelen JP, Wierenga RK. Structures of the “open” and “closed” state of trypanosomal triosephosphate isomerase, as observed in a new crystal form: implications for the reaction mechanism. Proteins. 1993; 16:311–326. [PubMed: 8356028]

72. Jogl G, Rozovsky S, McDermott AE, Tong L. Optimal alignment for enzymatic proton transfer: structure of the Michaelis complex of triosephosphate isomerase at 1.2-Å resolution. Proc Natl Acad Sci U S A. 2003; 100:50–55. [PubMed: 12509510]

73. Donnini S, Groenhof G, Wierenga RK, Juffer AH. The planar conformation of a strained proline ring: a QM/MM study. Proteins. 2006; 64:700–710. [PubMed: 16741995]

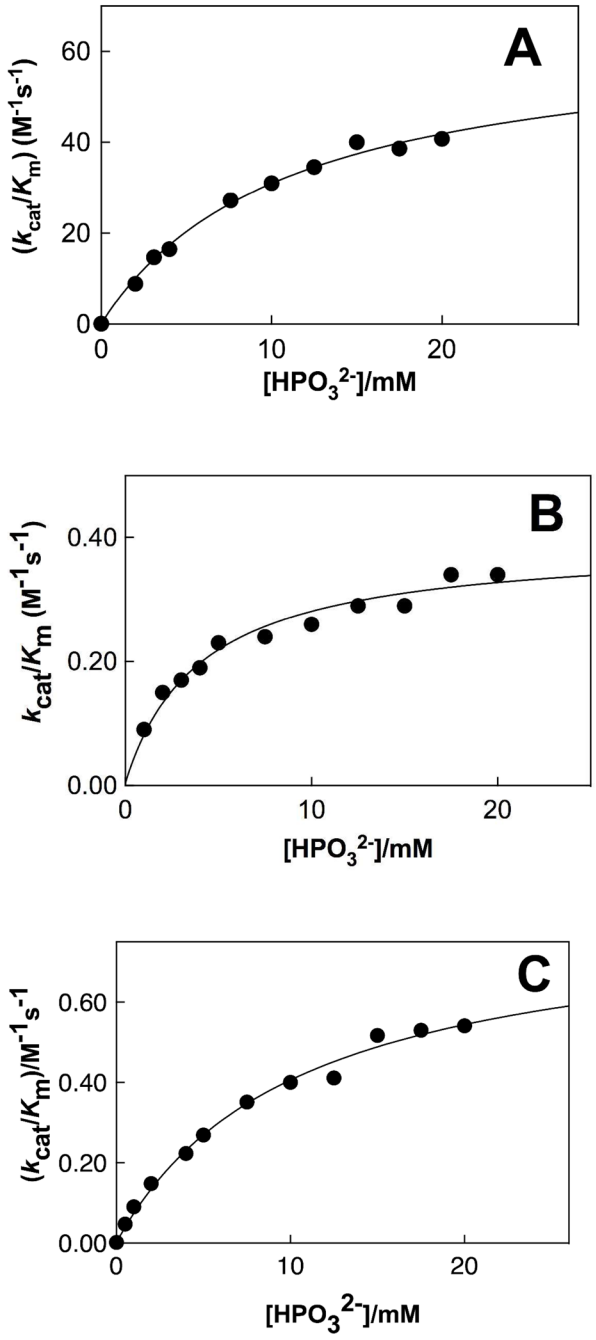

Figure 1.

Dependence of the second-order rate constants k_{cat}/K_m for the TIM-catalyzed turnover of the free carbonyl form of [1-^{13}C]-GA in D_2O on [HPO_3^{2-}] at pD 7.0 and 25 °C at I = 0.1, NaCl. The data were fit to eq 5 derived for the model shown in Scheme 3. A. Wildtype *c*TIM. B. L7RM *c*TIM. C. P168A *Tbb*TIM.

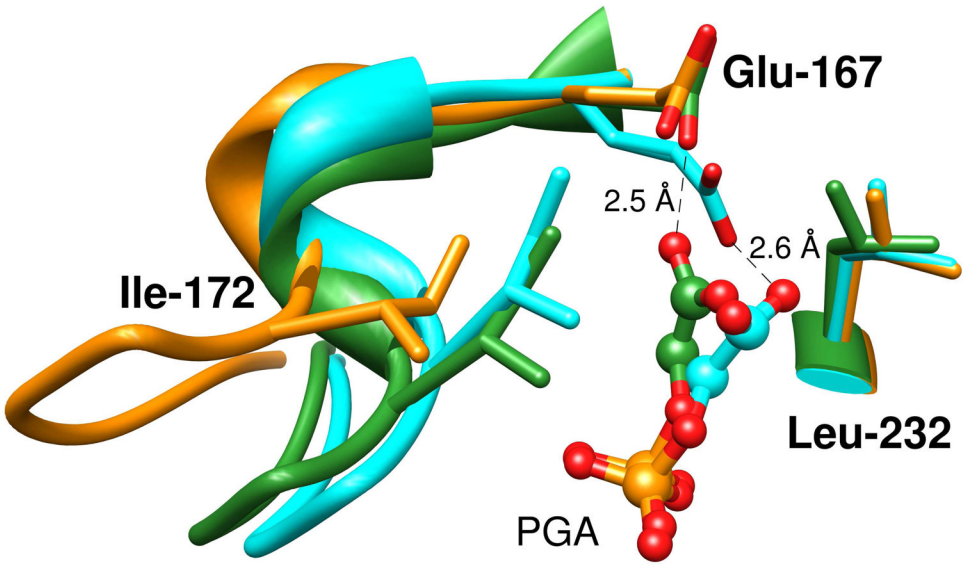

Figure 2.

Superposition of models, from X-ray crystal structures, which show the active sites of unliganded wildtype *Tbb*TIM (gold, PDB entry 5TIM), PGA-liganded TIM from *Leishmania mexicana* (cyan, PDB entry 1N55); and, PGA-liganded P168A mutant *Tbb*TIM (green, PDB entry 2J27). The ligand induced enzyme conformational changes are observed for wildtype and P168A mutant *Tbb*TIM are similar, except that the carboxylate side chain of Glu167 remains in open “swung-out” conformation at the P168A mutant.

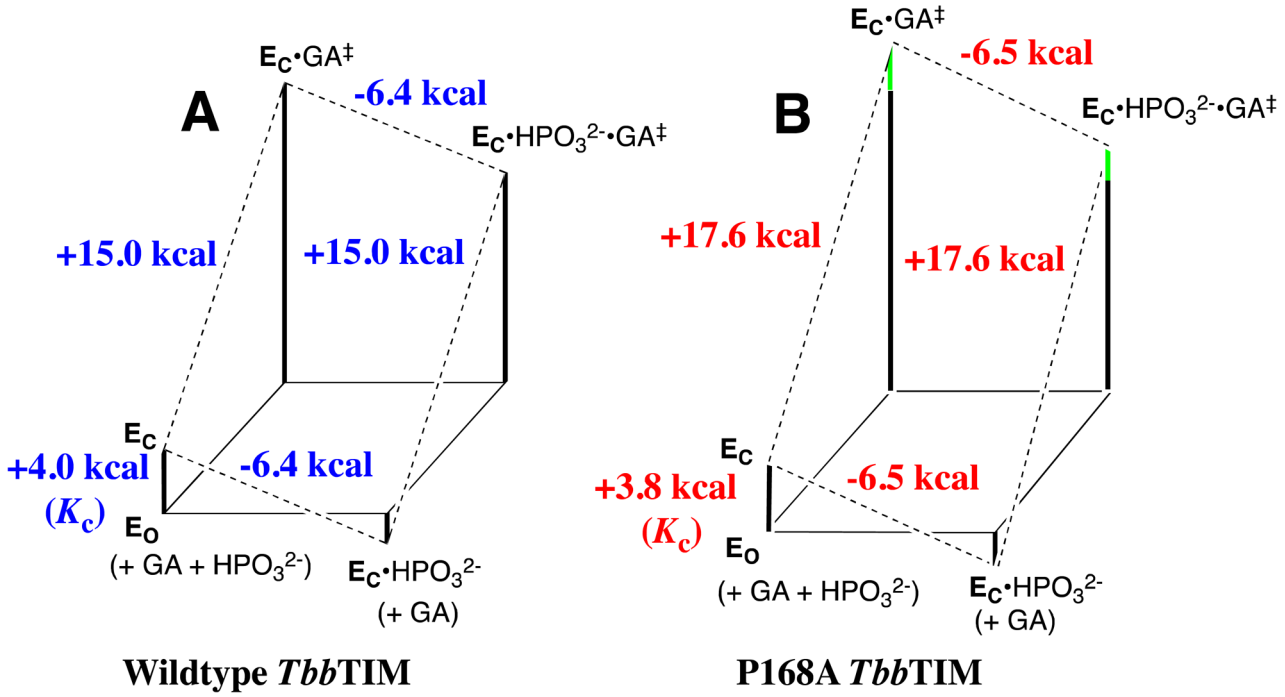

Figure 3.

Free energy profiles for turnover of GA by free TIM ($\mathbf{E_O}$) and by TIM that is saturated with HPO_3^{2-} ($\mathbf{E_C}$•HPO_3^{2-}), constructed for Scheme 5 using the kinetic parameters reported in Table 3. The profiles show the activation free energy changes calculated using the Eyring equation at 298 K for reactions catalyzed by wildtype and P168A mutant *Tbb*TIM. (A) Reactions catalyzed by wildtype *c*TIM. The difference between the total intrinsic phosphite dianion binding energy of −6.4 kcal/mol and ΔG^o = −2.4 kcal/mol for binding of HPO_3^{2-} to the inactive open enzyme $\mathbf{E_O}$ to give the active closed liganded enzyme $\mathbf{E_C}$•HPO_3^{2-} is attributed to ΔG_C = 4.0 kcal/mol for the conformational change that converts $\mathbf{E_O}$ to $\mathbf{E_C}$. (B) Reactions catalyzed by the P168A mutant. The observed barriers for conversion of $\mathbf{E_O}$ to the transition state for the unactivated and phosphite dianion activated reaction are 2.6 kcal/mol higher than for the wildtype *c*TIM catalyzed reaction (green bars, Figure 3B).

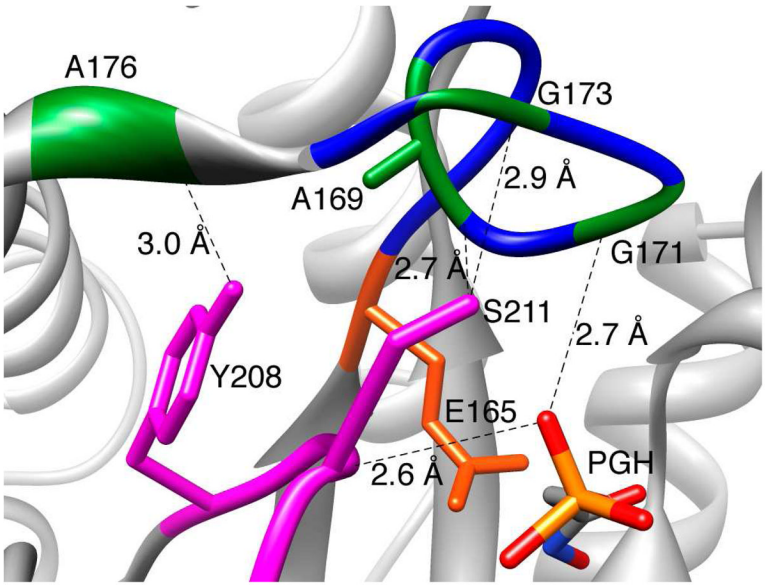

Figure 4.

Reprinted from Ref. 27. A representation of the structure of the closed form of TIM from chicken muscle in the region of the active site. This Figure shows the important interactions between flexible loop 6 (Pro166 to Ala176) and loop 7 (Tyr208 to Ser211), which form upon binding of PGH, an analog of the enediolate reaction intermediate (PDB entry 1TPH).[57,58] The 208-YGGS sequence was replaced by 208-TGAG at the loop 7 mutant of *c*TIM.

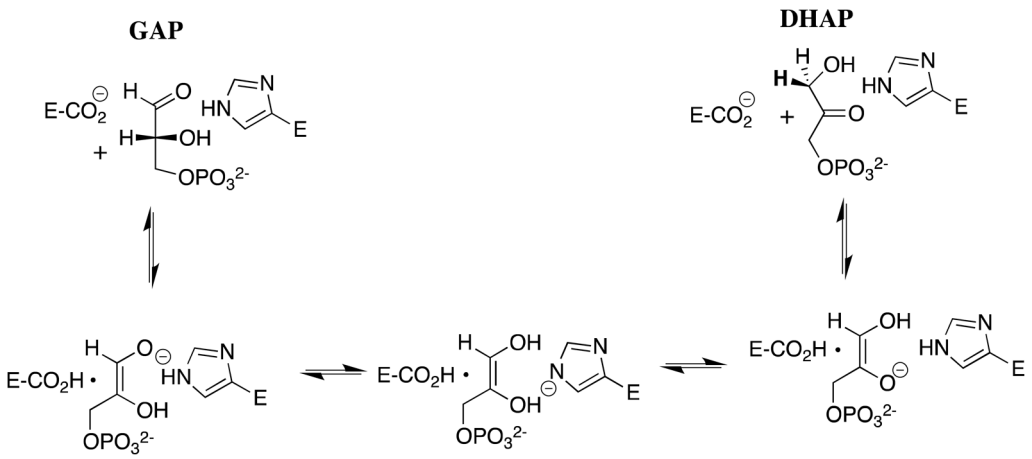

Scheme 1.

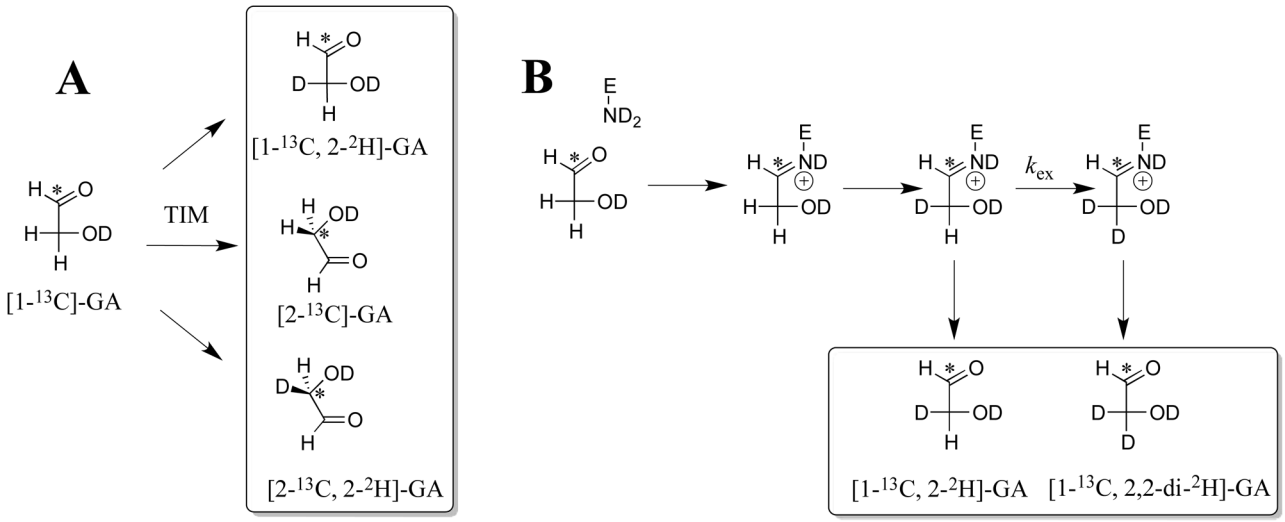

Scheme 2.

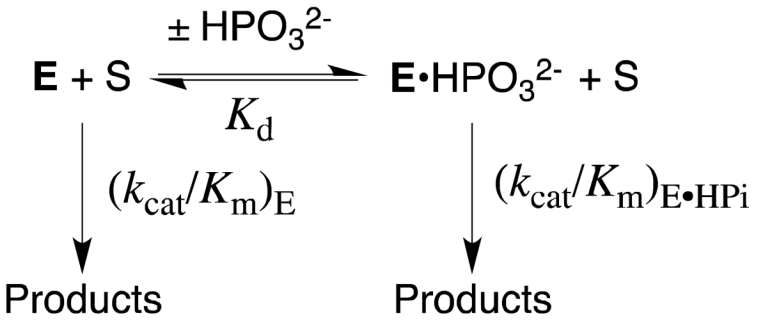

Scheme 3.

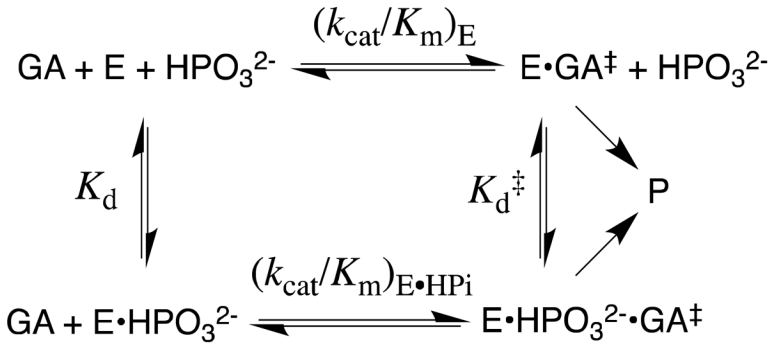

Scheme 4.

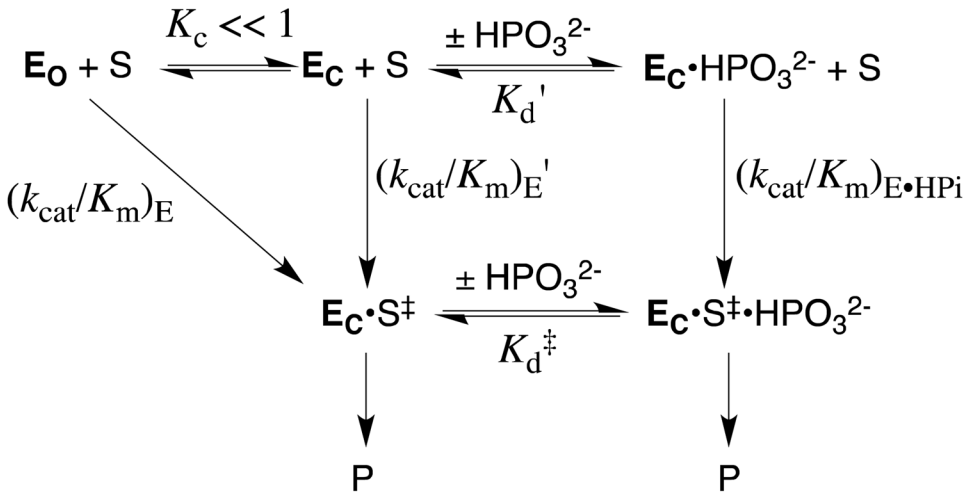

Scheme 5.

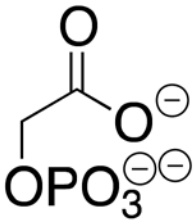

PGA

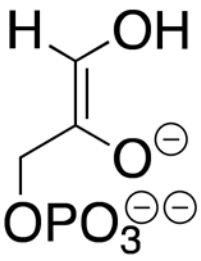

Enediolate Trianion

Chart 1.

Table 1

Kinetic Parameters For Isomerization of GAP and DHAP Catalyzed by Wildtype and Mutant Forms of Triosephosphate Isomerase from Chicken Muscle and *Trypanosoma brucei brucei* at pH 7.5 and 25 °C[a]

	GAP [b]				DHAP [c]			
TIM	k_{cat} (s^{-1})	K_m (mM)	k_{cat}/K_m (M^{-1} s^{-1})	K_i (mM) PGA[d]	k_{cat} (s^{-1})	K_m (mM)	k_{cat}/K_m (M^{-1} s^{-1})	K_i (mM) Arsenate[e]
Wildtype *c*TIM	3200 ± 100	0.29 ± 0.02	1.1×10^7	0.019 ± 0.001	340 ± 5	0.59 ± 0.05	5.8×10^5	9.6 ± 1.6
L7RM *c*TIM	16 ± 1	0.27 ± 0.02	5.9×10^4	2.3 ± 0.1	8.0 ± 0.5	4.0 ± 0.2	2.0×10^3	3.8 ± 0.3
Wildtype *Tbb*TIM [f]	2100	0.25	8.4×10^6	0.055 [g]	300	0.70	4.3×10^5	4.6
P168A *Tbb*TIM	24 ± 1	0.091 ± 0.005	2.6×10^5	0.14 ± 0.01	6.5 ± 0.1	0.49 ± 0.02	1.3×10^4	10 ± 1

[a] Under standard assay conditions of 30 mM triethanolamine buffer at pH 7.5, 25 °C and I = 0.1 (NaCl). The kinetic parameters have been calculated using the total concentration of the free carbonyl and hydrated forms of GAP or DHAP.

[b] The errors for TIM-catalyzed isomerization of GAP were determined from the average of kinetic parameters determined in two experiments.

[c] The errors for TIM-catalyzed isomerization of DHAP are the standard deviations determined from the nonlinear least squares fits of the kinetic data.

[d] The initial velocity of the isomerization of several concentrations of GAP was determined in the presence of 0.021 and 0.053 mM PGA for wildtype *c*TIM, 1.9 and 4.9 mM PGA for L7RM *c*TIM, and 0.13 and 0.39 mM PGA for P168A *Tbb*TIM.

[e] The initial velocity of the isomerization of several concentrations of DHAP was determined in the presence of 2, 5 and 10 mM arsenate.

[f] Data from Ref. 54 unless noted otherwise.

[g] Ref. 19.

Table 2

Second-Order Rate Constants for the Reactions of [1-^{13}C]-GA in D_2O Catalyzed by L7RM *c*TIM and P168A *Tbb*TIM in the Absence and Presence of Phosphite Dianion in D_2O at 25 °C[a]

L7RM *c*TIM					P168A *Tbb*TIM				
$[HPO_3^{2-}]$ (mM)	[TIM] (mM)	$\Sigma(f_P)_E$ [b]	$(k_{cat}/K_m)_{obs}$ [c] (M^{-1} s^{-1})	(k_{cat}/K_m)[d] (M^{-1} s^{-1})	$[HPO_3^{2-}]$ (mM)	[TIM] (mM)	$\Sigma(f_P)_E$ [b]	$(k_{cat}/K_m)_{obs}$ [c] (M^{-1} s^{-1})	(k_{cat}/K_m)[d] (M^{-1} s^{-1})
0	0.48	0.03 [e]	0.15	0.0045	0	0.22	0.02 [e]	0.07	0.0014
1.0	0.34	0.37	0.24	0.089	0	0.49	0.02 [e]	0.06	0.0012
2.0	0.52	0.64	0.24	0.15	0.5	0.35	0.43	0.11	0.047
3.0	0.37	0.59	0.28	0.17	1.0	0.30	0.60	0.15	0.090
4.0	0.24	0.59	0.32	0.19	2.0	0.25	0.70	0.21	0.15
5.0	0.21	0.59	0.39	0.23	4.0	0.20	0.65	0.34	0.22
7.5	0.30	0.61	0.40	0.24	5.0	0.12	0.71	0.38	0.27
10	0.17	0.65	0.40	0.26	7.5	0.12	0.70	0.50	0.35
13	0.14	0.61	0.47	0.29	10	0.080	0.71	0.57	0.40
15	0.15	0.62	0.46	0.29	13	0.070	0.66	0.62	0.41
18	0.10	0.63	0.54	0.34	15	0.060	0.67	0.77	0.52
20	0.090	0.61	0.56	0.34	18	0.060	0.70	0.75	0.53
20	0.10	0.59	0.58	0.34	20	0.14	0.80	0.68	0.54

[a] Determined by ^{1}H NMR analysis of the reaction of 20 mM [1-^{13}C]-GA in D_2O at pD 7.0 (20 mM imidazole), 25 °C and I = 0.1 (NaCl).

[b] The sum of the yields of the specific products [2-^{13}C]-GA, [2-^{13}C, 2-^{2}H]-GA, and [1-^{13}C, 2-^{2}H]-GA from the reaction of [1-^{13}C]-GA at the enzyme active site (Scheme 2A), taken from Tables S2 and S3 of the Supporting Information.

[c] Observed second-order rate constant for the TIM-catalyzed reactions of [1-^{13}C]-GA, calculated from the observed first-order rate constant using eq 2.

[d] Second-order rate constant for the specific TIM-catalyzed reaction of [1-^{13}C]-GA to give the products shown in Scheme 2A, calculated from $(k_{cat}/K_m)_{obs}$ for the disappearance of [1-^{13}C]-GA using eq 4.

[e] Calculated using the estimated yield of [1-^{13}C, 2-^{2}H]-GA formed by the specific reaction shown in Scheme 2A given in Tables S2 and S3 of the Supporting Information).

Table 3

Kinetic Parameters for the Unactivated and the Phosphite-Activated Reactions of the Free Carbonyl Form of [1-^{13}C]-GA Catalyzed by Wildtype and Mutant Forms of Triosephosphate Isomerase from Chicken Muscle and *Trypanosoma brucei brucei* in D_2O at 25 °C (Scheme 3)[a]

TIM	$(k_{cat}/K_m)_E$[b] (M^{-1} s^{-1})	$(k_{cat}/K_m)_{E\cdot HPi}$[c] ($M^{-1}$ s^{-1})	K_d[d] (mM)	$K_d^{\ddagger}$[e] (mM)	$\frac{(k_{cat}/K_m)_{E\bullet HPi}}{(k_{cat}/K_m)_E}$	$(k_{cat}/K_m)_{E\cdot HPi}/K_d$[f] ($M^{-2}$ s^{-1})
Wildtype *c*TIM	0.1 [g]	65 ± 4	11 ± 1.3	0.017	650	5900
L7RM *c*TIM	0.0045 (< 0.008) [h]	0.39 ± 0.02	4.1 ± 0.5	0.042	100	95
Wildtype *Tbb*TIM [i]	0.07	64	19	0.021	900	3400
P168A *Tbb*TIM	0.0013 (< 0.01) [h]	0.83 ± 0.05	10 ± 1.3	0.016	600	83

[a] Determined by ^{1}H NMR analysis of the reaction of 20 mM [1-^{13}C]-GA in D_2O at pD 7.0 (20 mM imidazole), 25 °C and I = 0.1 (NaCl).

[b] Second-order rate constant for the unactivated TIM-catalyzed reaction of [1-^{13}C]-GA in the absence of phosphite dianion.

[c] Second-order rate constant for the reaction of [1-^{13}C]-GA catalyzed by the phosphite-liganded enzyme.

[d] Dissociation constant for binding of phosphite dianion to the free enzyme.

[e] Dissociation constant for release of phosphite dianion from the transition state complex, calculated using eq 6 derived for Scheme 4.

[f] Third-order rate constant for the phosphite-activated TIM-catalyzed reaction of [1-^{13}C]-GA.

[g] Calculated from data reported in Ref. 49 (see Table S1 of the Supporting Information).

[h] Upper limit for $(k_{cat}/K_m)_E$, calculated using eq 4 with the assumption that [1-^{13}C, 2-^{2}H]-GA forms exclusively by the specific pathway shown in Scheme 2A.

[i] Data from Ref. 54.